A lattice dynamical treatment for the total potential energy of single-walled carbon nanotubes and its applications: relaxed equilibrium structure, elastic properties, and vibrational modes of ultra-narrow tubes

2008 J. Phys.: Condens. Matter 20 045228

(http://iopscience.iop.org/0953-8984/20/4/045228)

IOP PUBLISHING JOURNAL OF PHYSICS: CONDENSED MATTER

J. Phys.: Condens. Matter **20** (2008) 045228 (10pp) doi:10.1088/0953-8984/20/04/045228

A lattice dynamical treatment for the total potential energy of single-walled carbon nanotubes and its applications: relaxed equilibrium structure, elastic properties, and vibrational modes of ultra-narrow tubes

Jin-Wu Jiang[1], **Hui Tang**[1], **Bing-Shen Wang**[2] **and Zhao-Bin Su**[1,3]

[1] Institute of Theoretical Physics, Chinese Academy of Sciences, Beijing 100080, People's Republic of China
[2] State Key Laboratory of Semiconductor Superlattice and Microstructure and Institute of Semiconductor, Chinese Academy of Sciences, Beijing 100083, People's Republic of China
[3] Center for Advanced Study, Tsinghua University, Beijing 100084, People's Republic of China

E-mail: jwjiang@itp.ac.cn

Received 1 August 2007, in final form 16 November 2007
Published 11 January 2008
Online at stacks.iop.org/JPhysCM/20/045228

Abstract

In this paper, we propose a lattice dynamic treatment for the total potential energy of single-walled carbon nanotubes (SWCNTs) which is, apart from a parameter for the nonlinear effects, extracted from the vibrational energy of the planar graphene sheet. The energetics, elasticity and lattice dynamics are treated in terms of the same set of force constants, independently of the tube structures. Based upon this proposal, we have investigated systematically the relaxed lattice configuration for narrow SWCNTs, the strain energy, the Young's modulus and Poisson ratio, and the lattice vibrational properties with respect to the relaxed equilibrium tubule structure. Our calculated results for various physical quantities are nicely in consistency with existing experimental measurements. In particular, we verified that the relaxation effect makes the bond length longer and the frequencies of various optical vibrational modes softer. Our calculation provides evidence that the Young's modulus of an armchair tube exceeds that of the planar graphene sheet, and that the large diameter limits of the Young's modulus and Poisson ratio are in agreement with the experimental values of graphite; the calculated radial breathing modes for ultra-narrow tubes with diameters ranging between 2 and 5 Å coincide with the experimental results and the existing *ab initio* calculations with satisfaction. For narrow tubes with a diameter of 20 Å, the calculated frequencies of optical modes in the tubule's tangential plane, as well as those of radial breathing modes, are also in good agreement with the experimental measurements. In addition, our calculation shows that various physical quantities of relaxed SWCNTs can actually be expanded in terms of the chiral angle defined for the corresponding ideal SWCNTs.

1. Introduction

After the discovery of carbon nanotubes (CNTs) in 1991 [1], several methods have been developed for preparing CNTs with ultra-small diameters. Previously, CNTs were synthesized in free space [2, 3] and the quotient of narrow CNTs was quite low. Afterwards, Tang *et al* [4–7] initiated the growth of single-walled carbon nanotubes (SWCNTs) inside a channel

of zeolite template. SWCNTs prepared in this way have a diameter as small as 4.2 ± 0.2 Å. Actually, there are three kinds of tubes with different chiralities in this diameter range: (5, 0), (4, 2), and (3, 3). The fabrication process was further developed to prepare a type of sample with (5, 0) and (3, 3) chiralities only [8] with a very narrow diameter distribution. More recently, stable CNTs with a diameter of 3 Å is found inside a multi-walled carbon nanotube [9]. As is shown by density functional studies [9], this CNT might be interpreted as an armchair CNT (2, 2) with a radial breathing mode (RBM) at 787 cm^{-1}. All these technological improvements progressively stimulated experimental and theoretical studies on ultra-narrow SWCNTs [10–17].

Since the narrow CNTs possess largish curvatures, equilibrium geometries would deviate from the ideal geometry, i.e. deduced from a seamlessly rolled up planar graphitic lattice sheet referring to a chiral vector $\vec{R} = n_1\vec{a}_1 + n_2\vec{a}_2$ [18]. Various methods have been developed to determine the equilibrium geometry of free SWCNTs [10, 19–22]. Among others, in [10] the author calculated the total energy for narrow SWCNTs using a first-principles, all-electron, self-consistent local-density functional band-structure method. The calculated total energy can be parameterized in terms of five profitable parameters—i.e. generalized motif variables (GMVs)—with the line-group symmetry intimately retained. The equilibrium geometry is obtained by an optimization procedure with respect to these GMVs. In [20], a molecular mechanical model for the effective total potential energy is proposed to calculate the equilibrium structure and the strain energy of achiral SWCNTs that is a quadratic form of lattice site displacements with respect to the planar graphite sheet. Apart from deviations of three bond lengths and three bond angles, a pyramidalization angle is introduced to describe the energy associated with the curvature. The calculated results are consistent with existing numerical results based on *ab initio* calculations.

Moreover, based upon the relaxed equilibrium geometry provided by the *ab initio* method [10], Milošević *et al* [11] applied the line-group symmetry-based force constant method to calculate the vibrational modes of ultra-narrow SWCNTs, in which the fitted force constants of narrow SWCNTs have been adjusted with respect to the provided cylindrical web geometry.

Besides, the elastic properties for carbon nanotubes have stimulated a large number of experimental and theoretical studies [23]. In particular, the Young's modulus is a significant physical quantity which reflects the striction of equilibrium structure in response to the load that is impressed. In [24], the axial Young's modulus of the SWCNT is measured as 1.2 TPa by the atomic force microscope technique. By observing their free-standing room-temperature vibrations in a transmission electron microscope [25], the Young's moduli for 27 nanotubes in the diameter range 10–15 Å were measured, and the average Young's modulus is 1.25 − 0.35/+0.45 TPa [26]. An interesting fact was acknowledged that the Young's modulus of certain nanotubes is even higher than that of bulk graphite.

There have been a large number of theoretical calculations for the Young's modulus and the Poisson ratio. Taking 3.4 Å as the thickness of the SWCNTs, the *ab initio* method [21, 27, 28], tight-binding approximation [29, 30], and force constant model [31] gave results for Young's modulus with a range from 1 to 1.24 TPa, and for the Poisson ratio in a range of 0.16–0.27. In [32–36], the calculated Young's modulus is about 5 TPa with a thickness of 0.7 Å. The above calculated results show up only a slight dependence on the radii and chiralities. However, in [37–42], the calculated Young's modulus or the Poisson ratio are found to be chirality and tube radius-dependent. In [37], the Poisson ratio of armchair tubes has a value larger than that of a planar graphene sheet, while for a zigzag tube it is smaller, and its planar sheet limit is 0.21. In [38, 39, 41], the Poisson ratio decreases with increasing tube diameter and has an upper limit to the diameter of 0.16. Anyhow, to our knowledge the resolution of the experimental measurements for the Young's modulus and Poisson ratio is still not yet satisfactory enough and the various correspondending theoretical calculations are even more diverse.

As we have seen above, *figuring out the total potential energy of SWCNTs as a functional of the cylindrical lattice configuration is the key issue underlying the investigation of the equilibrium structure, strain energy, Young's modulus and lattice dynamics of ultra-narrow tubes.*

In this paper, we propose that the total potential energy for SWCNTs can be extracted from the vibrational energy of the planar graphene sheet with five force constants. In this, the bi-linear forms of the lattice site displacements are accounted for by the equilibrium lattice configuration of the planar graphite as the reference point, while one of the potential terms for the twist motion needs to be improved by including a quartic term to account for the nonlinear effect. One of the advantages of our proposal is that the equilibrium structure, the elasticity, and the lattice dynamic properties for all kinds of SWCNTs are calculated in terms of the same set of six (5 + 1) force constants, which essentially reflects a unified microscopic mechanism founded on the five forms of motion of the graphite-type cylindrical lattice sheet. Based upon this proposal, we have investigated systematically the relaxed lattice configuration for narrow SWCNTs, the strain energy, the Young's modulus and the Poisson ratio, and the lattice vibrational properties with respect to the relaxed equilibrium tubule structure. The calculated results are nicely in consistency with the existing experimental measurements.

In section 2, the total potential energy for SWCNTs is presented, and the relaxed equilibrium geometry and corresponding strain energy are discussed. Section 3 is devoted to the lattice dynamics for ultra-narrow SWCNTs, while section 4 is devoted to the Young's modulus and the Poisson ratio. Finally, the conclusion is in section 5.

2. The relaxed equilibrium structure

2.1. The geometry

We recall the geometrical description for the relaxed equilibrium structure of SWCNTs, in particular for ultra-narrow tubes, following [10]. As for the cylindrical coordinate

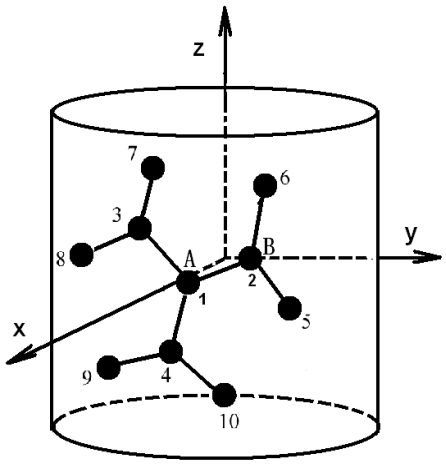

Figure 1. Sketch of carbon atoms on a cylindric surface.

description shown in figure 1, we first set the z axis to be along the tube axis, while the x axis is fixed to pass through one of the A atoms. We further introduce a planar image of the cylindrical lattice sheet by unfolding the cylindrical tube into a planar lattice sheet, which is actually a tangential plane with the tangent line as a generatrix passing through the A atom, and set atom A as the origin of the plane with coordinates of $(r_A, 0, 0)$, where r_A is the radius of atom A. The planar lattice sheet is constituted of parallelogram primitive cells with $\vec{a}_1$ and $\vec{a}_2$ as its basic vectors. The deviations of CNTs with relaxed geometry from that of ideal geometry can be illustrated most conveniently by the primitive cells on the image plane. For that of ideal geometry, the basic vectors are of equal magnitude, with an intra-angle of $\pi/3$ between themselves, while for those of relaxed geometry, their magnitudes are no longer equal and the angle can deviate from $\pi/3$. Meanwhile, the location of the in-cell B atom relative to A atom can also deviate from that of the ideal geometry.

Now we introduce the chiral vector $\vec{R} = n_1\vec{a}_1 + n_2\vec{a}_2$ initiated from the atom A along the y axis in the image sheet, where R is the image circumference of a cylindrical lattice sheet. We then introduce a screw vector $\vec{H} = p_1\vec{a}_1 + p_2\vec{a}_2$, with integers p_1 and p_2 satisfying $p_1n_2 - p_2n_1 = N$ and N being the largest common divisor of the integer pair (n_1, n_2). Exactly following [10] and [18], $\vec{H}$ and $\frac{\vec{R}}{N}$ constitute the basic ingredients of the generalized motif cell, upon which a generalized screw operation $S(\alpha, h)$ and a generalized N-fold rotation operation C_N can be established. The former is a rotation α around the tube axis with a simultaneous translation h along the tube axis; the latter is a rotation of $\frac{2\pi}{N}$ around the tube axis. A generalized motif cell labeled (m, l) can be generated from the $(0, 0)$ cell by successive operations of $S(\alpha, h)$ and C_N for m and l times, respectively. For the in-cell geometry of a generalized motif cell, originating from atom A the position of atom B can be fixed by a rotation α' around the tube axis and two simultaneous translations h' and $(r - r_A)$ along the tube axis and the tube radius, respectively.

As a result, the coordinates on the cylindrical lattice sheet for each site (m, l, s) with $s = $ A, B can be expressed as

$$\begin{aligned}
&\vec{r}(m, l, s) = (r_s \cos\phi, r_s \sin\phi, z),\\
&r_s = r_A, \qquad \phi = m\alpha + \frac{l}{N}2\pi,\\
&\quad z = mh \qquad (\text{for A}),\\
&r_s = r, \qquad \phi = m\alpha + \frac{l}{N}2\pi r + \alpha',\\
&\quad z = mh + h' \qquad (\text{for B}).
\end{aligned} \tag{1}$$

Meanwhile, the corresponding coordinates in the image plane have the form

$$\vec{r}^{\,\text{image}}(m, l, s) = (r_s, \phi r_s, z) \tag{2}$$

with the x-components of both A and B atoms being constants, respectively.

Therefore, the six GMVs (r, r_A, α', h', α, and h) provide a complete description for the geometry of the lattice structure of SWCNTs, in which all the A and B atoms are allowed to sit on different cylindrical surfaces with radii r_A and r, respectively.

2.2. The total potential energy

In fact, in the sense of a quadratic approximation, the vibration potential of the single-layer graphite lattice sheet provides a proper description of various modalities of lattice motion. We therefore propose that the total potential energy of SWCNTs can be extracted from the vibration potential of a graphene lattice sheet [43][4] as follows. First, the total potential energy contributed by carbon atom 1, i.e. atom (0, 0, A), is composed of the following five terms in which a local planar graphene sheet is taken as the reference point:

$$U_A = V_l + V_{sl} + V_{BB} + V_{rc} + V_{tw}, \tag{3}$$

where V_l and V_{sl} are the potentials of the spring forces between the nearest-neighbor and the next-nearest-neighbor atom pair, respectively, as shown in figure 1, V_{BB} is the energy associated with bond angle variations, V_{rc} describes out-of-surface bond bending, i.e. a kind of strain force on atom i in the out-of-surface direction from its three nearest neighbors in the curling process, and V_{tw} is the twist potential energy:

$$V_l = \frac{k_l}{4}\sum_{i=2}^{4}[(\Delta\vec{r}_i - \Delta\vec{r}_1)\cdot\vec{e}^{\,l}_{1i}]^2, \tag{4}$$

$$V_{sl} = \frac{k_{sl}}{4}\sum_{j=5}^{10}[(\Delta\vec{r}_j - \Delta\vec{r}_1)\cdot\vec{e}^{\,l}_{1j}]^2, \tag{5}$$

$$V_{BB} = \frac{k_{BB}}{2}\sum_{\eta=1}^{3}(\cos\Theta_\eta - \cos\Theta_0)^2, \tag{6}$$

[4] There are slight differences between our five force constants and those of Aizawa *et al*, which does not make sense for a description of the lattice dynamics of planar graphene sheet.

$$V_{\rm rc} = \frac{k_{\rm rc}}{2}\left[\left(\sum_{i=2}^{4}\Delta\vec{r}_i - 3\Delta\vec{r}_1\right)\cdot\vec{e}_1^{\,r}\right]^2, \tag{7}$$

$$V_{\rm tw} = \frac{k_{\rm tw}}{4}\sum_{\langle i,j\rangle} f(x_{ij}^1), \tag{8}$$

$$x_{ij}^1 = [(\Delta\vec{r}_i - \Delta\vec{r}_j) - (\Delta\vec{r}_{i'} - \Delta\vec{r}_{j'})]\cdot\vec{e}_{1k}^{\,r},$$

$$f(x) = \begin{cases} x^2 - K_{\rm ah}x^4, & \text{if } |x| < \sqrt{\frac{1}{2K_{\rm ah}}}, \\ \dfrac{1}{4K_{\rm ah}}, & \text{if } |x| \geqslant \sqrt{\frac{1}{2K_{\rm ah}}}. \end{cases}$$

In equations (4) to (8), $i = 2, \ldots, 4$ and $j = 5, \ldots, 10$ are the nearest-and next-nearest neighbors of atom 1 respectively, Θ_η with $\eta = 1, 2, 3$ represent the three bond angles with atom 1 as the common apex while $\Theta_0 = \frac{2\pi}{3}$ is the bond angle in the graphic plane, $\langle i, j\rangle$ represents a pair of atoms that are the nearest neighbors to atom 1 with k being the third of its nearest neighbors, and the pair $\langle i', j'\rangle$ is the image of $\langle i, j\rangle$ referring to a C_2 rotation around the axis in $\vec{e}_{1k}^{\,r}$. Moreover,

$$\Delta\vec{r}_i = \vec{r}_i - \vec{r}_i^{\,0} \tag{9}$$

is the displacement of the carbon atom i from the planar graphene sheet $\vec{r}_i^{\,0}$ to its counterpart in the tubal lattice sheet $\vec{r}_i$, in which i stands for the site index (m, l, s) defined on the cylindrical lattice sheet. In addition, $\vec{e}_{1i}^{\,l} = \frac{\vec{r}_i^{\,0} - \vec{r}_1^{\,0}}{|\vec{r}_i^{\,0} - \vec{r}_1^{\,0}|}$ is the unit vector pointing from atom 1 to atom i in the graphite sheet, and $\vec{e}_i^{\,r}$ and $\vec{e}_{1k}^{\,r}$ are vertical unit vectors of the planar graphene sheet located at the site i and the middle point of sites 1 and k of the graphene sheet, respectively. All the unit vectors are defined on the local reference graphene sheet and are introduced to keep the rigid rotational invariance symmetry. The above five potential terms in principle cover the main features of the modalities of lattice deformation suggested by Shen *et al* [20, 38], Chang *et al* [39] in their mechanical model.

Correspondingly, that part of total potential energy in association with carbon atom B $(0, 0, \mathrm{B})$ has a similar expression to that of $U_{\rm A}$, but with its geometrical parameters replaced by the counterpart of atom B.

Second, we express the lattice displacements in $U_{\rm A}$ and $U_{\rm B}$ in terms of the generalized motif variables. This spells out that the locally constructed $(0, 0)$ generalized motif cell with a pair of carbon atoms A and B can continue to form a whole seamlessly closed cylindrical lattice sheet in which the generalized screw as well as rotation symmetries are inherited. As a result, the total potential energy of SWCNTs has the form of a simple multiple of those potential energies associated with a pair of nearest-neighboring atoms A and B, i.e. $U_{\rm A}$ and $U_{\rm B}$ respectively,

$$U_{\rm t} = \mathcal{N} * (U_{\rm A} + U_{\rm B}), \tag{10}$$

where $\mathcal{N}$ is the number of generalized motif cells of SWCNTs under consideration. The redundant counting in the total potential energy contributed by different carbon atoms can be accounted for by an appropriate re-setting for the values of the relevant force constants. We further address that this sort of parameterization procedure can be carried out for all kinds of SWCNTs, including both chiral and achiral tubes.

The values of the force constants are $k_{\rm l} = 305\ \mathrm{N\,m^{-1}}$, $k_{\rm sl} = 68.25\ \mathrm{N\,m^{-1}}$, $k_{\rm BB} = 1.38\times10^{-11}$ erg, $k_{\rm rc} = 14.8\ \mathrm{N\,m^{-1}}$, $k_{\rm tw} = 6.24\ \mathrm{N\,m^{-1}}$, and $K_{\rm ah} = 2.5\ \mathrm{\AA^{-2}}$. The frontal five force constants come from vibration energy of the planar graphene sheet [43] (see footnote 4). Since the twisting deformations increase substantially with decreasing tube diameter—for example, the twisting angle for the C–C bond can take a value as large as 26° for the narrow SWCNT (6, 3)—an additional force constant for the anharmonic improvement of $K_{\rm ah}$ in equation (8) has to be introduced. We notice here that the differences in lattice dynamics between two such types of system are essentially due to their different spatial geometries, which are characterized by their own equilibrium lattice structure.

2.3. The relaxed structure of SWCNTs

We introduce the total potential energy per atom, U, as

$$U = U(r, r_{\rm A}, \alpha, h, \alpha', h') = (U_{\rm A} + U_{\rm B})/2. \tag{11}$$

By minimizing $U(r, r_{\rm A}, \alpha, h, \alpha', h')$ with respect to the six GMVs, we obtain the optimized equilibrium geometry described by the GMVs $(\bar{r}, \bar{r_{\rm A}}, \bar{\alpha}, \bar{h}, \bar{\alpha'}, \bar{h'})$ as well as the strain energy $U_{\rm s} = U(\bar{r}, \bar{r_{\rm A}}, \bar{\alpha}, \bar{h}, \bar{\alpha'}, \bar{h'})$. It is interesting to address that the optimized equilibrium lattice configurations for all tubes are shown to be $\bar{r_{\rm A}} = \bar{r}$. This is because the total energy $U_{\rm t}$ remains unchanged when the tube is rotated upside down with atoms A and B mutually permuted, so the optimized geometry must exhibit C_2 symmetry. The reflected symmetry $\sigma_{\rm h}$ with respect to the cross section is also maintained for achiral tubes.

The various calculated lattice structure properties and strain energies for narrow SWCNTs with a diameter of [2.6, 5] Å are listed in table 1, where the calculated GMVs are comparable to those from *ab initio* calculations [10]. Moreover, it is shown that the curvature energy associated with the fourth potential energy term in equation (7) dominates the total strain energy, while the corresponding contributions from the bond variation are usually much less than those from the bond angle variations (see table 2). For a closer examination, we find that the optimized carbon–carbon bond lengths deduced from the parameters in table 1 for tubes (5, 0), (4, 2), (3, 3) are about 9% larger than the *ab initio* results in [10]. We understand that such a discrepancy is essentially due to the treatment of the next-neighbor potential energy. If we artificially ignore this potential energy term, the resulting bond lengths will meet those of the *ab initio* calculations. This result is consistent with the corresponding results in [44], where the next-neighbor potential energy favors increasing bond lengths.

In [40], it is reported that the strain energy varies with tubule radius as $\frac{1}{r^2}$ by applying the Tersoff–Brenner interatomic potentials. Here we plot the strain energy versus the radius in figure 2, which is comparable with the existing result [21, 40] and can be fitted well by $E_{\rm s} = \frac{c_1}{r^2} + \frac{c_2}{r^4}$, in consistency with the result of [20]. The coefficient of $\frac{1}{r^4}$—i.e. c_2—is a bit large. This is because, in [20], there is no such twisting energy term that we have.

Table 1. The calculated results for the five GMVs with $r_A = \bar{r}$ and the strain energy for narrow SWCNTs.

(n_1, n_2)	r (Å)	α' (rad)	h' (Å)	α (rad)	h (Å)	E_s (eV)
(2, 2)	1.743	1.1036	0.000	1.5708	1.255	1.5596
(3, 1)	1.817	1.0019	0.337	4.5923	0.580	1.7596
(4, 0)	1.977	0.7854	0.613	0.7854	2.033	1.3636
(3, 2)	2.013	0.8460	0.148	2.4777	0.491	0.7977
(4, 1)	2.129	0.7512	0.416	4.9317	0.455	0.8171
(3, 3)	2.281	0.7088	0.000	1.0472	1.238	0.4522
(5, 0)	2.283	0.6283	0.652	0.6283	2.069	0.6484
(4, 2)	2.333	0.6788	0.250	2.0127	0.803	0.4781
(5, 1)	2.458	0.6075	0.475	5.1657	0.376	0.4606
(4, 3)	2.593	0.6000	0.112	1.7827	0.351	0.3083
(6, 0)	2.617	0.5236	0.672	0.5236	2.089	0.3759
(5, 2)	2.673	0.5652	0.324	2.6560	0.339	0.3163

Table 2. Contributions of five potential energy terms to the strain energy for tube (3, 3).

(3, 3)	V_l	V_{sl}	V_{BB}	V_{rc}	V_{tw}
(eV)	0.029 34	0.071 91	0.029 72	0.301 79	0.019 48

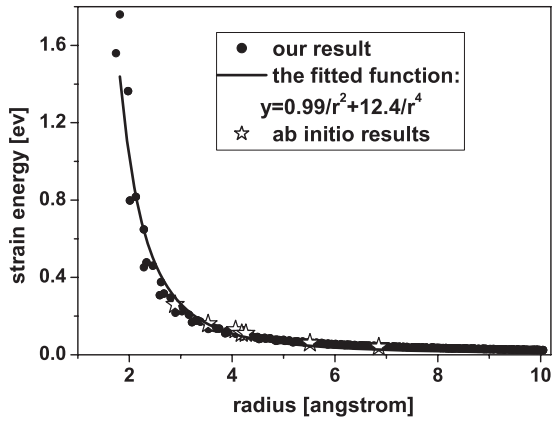

Figure 2. The strain energy as a function of radius for all tubes in [1.3, 10.0] Å. This is compared with the *ab initio* calculations [20, 21].

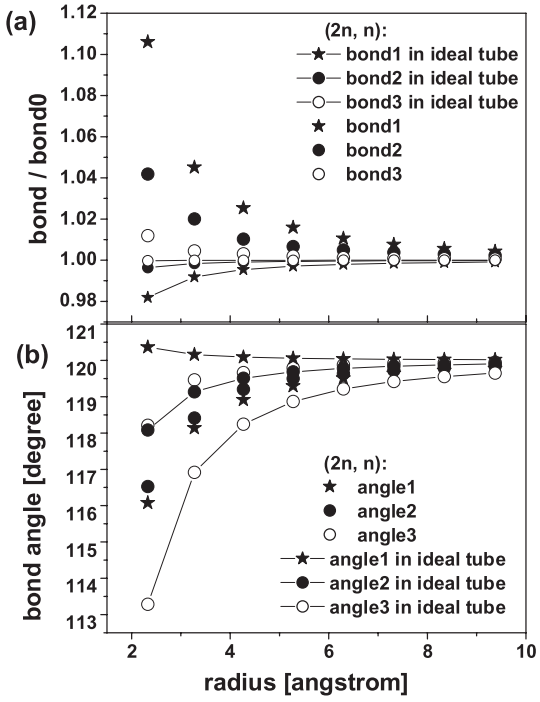

Figure 3. The reduced C–C bond lengths from that of graphite and the bond angles for different chiral tubes $(2n, n)$ with the relaxed geometry and the ideal geometry. Bond1, bond2, and bond3 are the bonds between atom 1 and atoms 2, 3, and 4 in figure 1, respectively. Bond angle i $(i = 1, 2, 3)$ is the angle opposite bond i.

Our calculation shows that the radius and C–C bond lengths of CNTs for the optimized lattice configuration are always larger than those of the corresponding CNTs for the ideal geometry. In figure 3(a), we display the three bond lengths representatively in units of the graphene bond length, 1.42 Å, for $(2n, n)$ tubes, with the relaxed geometry as well as the ideal geometry. The relaxation, resulting from the optimization procedure, would disentangle the warping-induced tension and make the inter-atomic bond length longer. To be precise, the bond lengths of the optimized lattice configuration decrease with increasing diameter and maintain values always larger than that of the graphene sheet. In contrast, for tubes of ideal geometry the bond lengths increase with increasing diameter and maintain values always smaller than that of the graphene sheet. As we can see in figure 3(a), one of the bond lengths of the tube (4, 2) is 1.39 Å for the ideal geometry, while it is 1.57 Å for the case of relaxed geometry, which is about 11% more than that of the graphene sheet.

As shown in figure 3(b), deviations of the bond angles from those of graphene are really considerable for narrow tubes with a diameter smaller than 8 Å. On the other hand, as can be seen in the same figure, this effect decreases quickly with increasing tube diameter.

3. Calculation results and discussion of phonon dispersion

In section 2, the relaxed equilibrium lattice configurations of SWCNTs are derived using an optimization procedure applied

Table 3. The values of two optical modes in the tangential plane from our calculation compared with the experimental results [46].

Optical mode	(11, 10)	(17, 9)	(27, 4)	(15, 14)
Calculated result	1597.3	1600.5	1602.5	1602.1
	1600.7	1603.6	1605.5	1603.7
Experiment [46]	1566(7)	1572(13)	1577.5(10)	1573(7)
	1593.5(6)	1591(8)	1593(5)	1592(5)

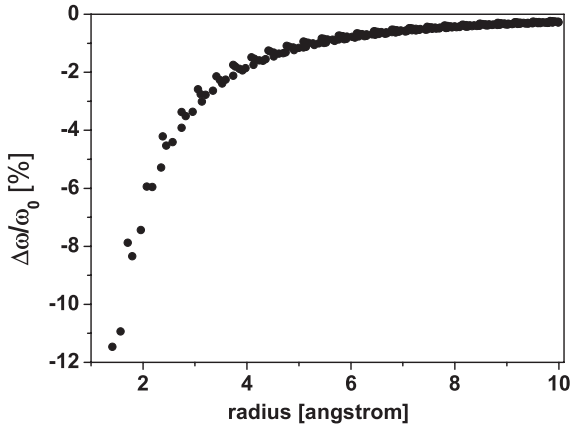

Figure 4. The dependence on radius of the relative frequency change due to the relaxation effect for the optical mode along the z axis. The small waviness of the line shows the dependence of the frequencies on the chiral angle. For chiral and zigzag tubes, this mode is the Raman-active mode.

to the proposed total potential energy. The vibrational potential of SWCNTs is actually caused by the deviation of lattice sites with respect to the relaxed equilibrium lattice configuration. It is obvious that the vibrational potential of SWCNTs would take the same form as the total potential energy, whereas the equilibrium position of the lattice site in the planar graphene sheet is therefore replaced by those in the relaxed cylindrical lattice sheet; meanwhile, the nonlinear term is no longer needed. The detailed modifications are as follows:

(1) $\Delta\vec{r}_i = \vec{r}_i - \vec{r}_{i0}$ is renamed by convention as the vibrational displacement $\vec{u}_i$ with $\vec{r}_{i0}$ the local planar graphene sheet to be replaced by the relaxed equilibrium position of atom i in the SWCNTs;

(2) $\cos\Theta_0$ in equation (6) is no longer the bond angle for the graphene sheet of $\frac{2}{3}\pi$ but the corresponding bond angle for the relaxed equilibrium configuration, which depends on distinct adjacent atom pairs that are nearest neighbors to the common apex atom i;

(3) $\vec{e}^{\,l}_{1i}$ and $\vec{e}^{\,l}_{1j}$ are kept as the unit vectors pointing from atom i and j to atom 1, respectively. $\vec{e}^{\,r}_1$ is replaced by $\vec{e}^{\,rc}_1 = -\frac{\sum_{i=2}^{4}\vec{r}_{i0}}{|\sum_{i=2}^{4}\vec{r}_{i0}|}$ and $\vec{e}^{\,r}_{1k}$ now becomes the unit vector along the radial direction of the mid-point of atoms 1 and k. We stress that all these unit vectors are defined on the cylindrical lattice sheet with the optimized equilibrium geometry, which *plays a crucial role* in keeping rigid rotational invariance for the vibrational potential of relaxed SWCNTs;

(4) The coefficient $K_{\rm ah}$ is taken to be zero.

Table 4. The values of RBM from our calculation compared with the experiments or other calculations.

RBM	(2, 2)	(5, 0)	(3, 3)	(4, 2)
Calculated result	804.3	561.3	550.8	538.6
Comparison	(787)[a]	(550)[b]	/	(510)[b]
RBM		(11, 10)	(16, 7)	(15, 6)
Calculated result		160.0	142.5	155.2
Comparison		(169.5(7))[c]	(154(5))[c]	(166(1))[c]

[a] The *ab initio* calculations from [9].
[b] The experimental results from [8].
[c] The experimental results from [46] and [47].

We emphasize here that *the five force constants of the above proposed quadratic vibrational energy are the same as those in* section 2.2. *They are applied to all kinds of SWCNT including those with small radii.* This is because the rigid rotation symmetry of the SWCNTs is kept precisely. Also, the curvature effect for the vibrational modes has been properly taken care of by the quadratic expression introduced above.

It is straightforward that such an obtained vibrational potential can again be parameterized in terms of the GMVs. Taking the advantage of the GMV description for the cylindrical lattice configuration, the underlined generalized screw and rotation symmetries ensure that the lattice dynamic equation, even for tubes with relaxed geometry, can be decomposed into a six-dimensional eigenvalue problem and becomes treatable.

For tubes with diameters from 2.8 to 25 Å, we calculate all the Raman- and infrared-active modes [45], and the velocities for the twisting (TW) and the longitude acoustic (LA) modes.

The relaxation effect for the non-zero vibrational modes of the tubes with relaxed geometry exhibits itself as a frequency lowering (mode softening) in comparison with their counterpart for tubes of ideal geometry. The effect of the relaxation on the optical mode along the z axis is shown in figure 4. The relaxation softens this mode considerably for narrow tubes. For example, for tubes with a radius as narrow as 2 Å, this mode is softened by as much as 8% relative to that of the ideal geometry.

The calculated frequencies for the optical mode in the tubal tangential plane coincide excellently with the experimental measurements on tubes (11, 10), (17, 9), (27, 4), (15, 14) [46]; see table 3. For the RBM, the calculated results from our model are in good agreement with the correspondent results from the experiments on tubes (5, 0), (4, 2), (11, 10), (16, 7), (15, 6) listed in table 4. Also, for the tube (2, 2), the calculated result is consistent with that of the *ab initio* calculation [9] (see table 4). Moreover, it can be seen from table 4 that the smaller tube has the larger RBM frequency. This is consistent with some other calculation results [8, 11].

Table 5. Polarization vectors $\vec{u} \equiv (\vec{u}(A), \vec{u}(B))$ as functions of r ($r \in [1.3, 10.0]$ Å) and θ, where $\vec{u}(A)$ and $\vec{u}(B)$ indicate the displacement vectors of atoms A and B in the (0, 0) unit cell, respectively. For the three modes in this table, $u_r(B) = u_r(A)$, $u_\phi(B) = -u_\phi(A)$, $u_z(B) = -u_z(A)$.

$(\kappa, n) = (0, 0)$		Vector(θ)	$f_i(r)$
R_1 (RBM)	$u_r(A)$	$f_0(r)$	$f_0(r) = 0.7072 - \frac{0.0026}{r^2}$
	$u_\phi(A)$	$f_1(r)\sin 3\theta$	$f_1(r) = -\frac{0.0212}{r} + \frac{0.1111}{r^2}$
	$u_z(A)$	$f_1(r)\cos 3\theta$	$f_1(r) = -\frac{0.0344}{r} + \frac{0.2167}{r^2}$
R_2 ($\vec{e}_\phi$ OP)	$u_r(A)$	$f_1(r)\sin 3\theta$	$f_1(r) = \frac{0.0211}{r} - \frac{0.1064}{r^2}$
	$u_\phi(A)$	$f_0(r) + f_1(r)\cos 12\theta$	$f_0(r) = 0.6975 + \frac{0.0313}{r^2}$, $f_1(r) = 0.0084 - \frac{0.0248}{r^2}$
	$u_z(A)$	$f_1(r)\sin 6\theta + f_2(r)\sin 12\theta$	$f_1(r) = 0.1642 - \frac{0.3742}{r^2}$, $f_2(r) = -0.0283 + \frac{0.1512}{r^2}$
R_3 ($\vec{e}_z$ OP)	$u_r(A)$	$f_1(r)\cos 3\theta$	$f_1(r) = \frac{0.0348}{r} - \frac{0.2189}{r^2}$
	$u_\phi(A)$	$f_1(r)\sin 6\theta + f_2(r)\sin 12\theta$	$f_1(r) = 0.1643 - \frac{0.3759}{r^2}$, $f_2(r) = -0.0283 + \frac{0.1510}{r^2}$
	$u_z(A)$	$f_0(r) + f_1(r)\cos 12\theta$	$f_0(r) = 0.6975 + \frac{0.0299}{r^2}$, $f_1(r) = 0.0084 - \frac{0.0236}{r^2}$

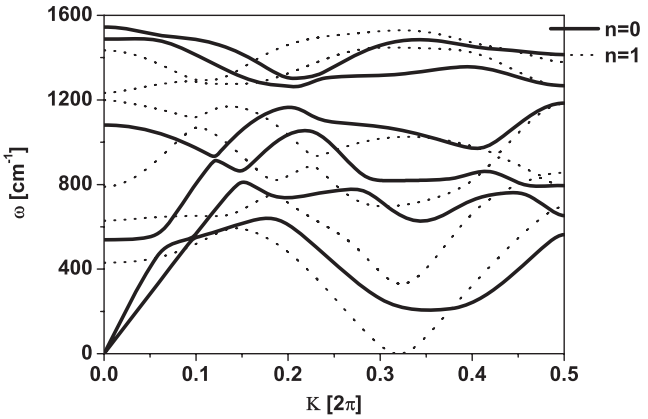

Figure 5. Phonon dispersion curves for SWCNT (4, 2) in the representation of helical and rotational quantum numbers. The flexure mode—i.e. the transversal acoustic mode—shows up at $(\kappa, n) = (\alpha, 1)$, where α is in the unit of 2π. It is doubly degenerate.

We take SWCNT (4, 2) as a typical example of a narrow tube. Its dispersion is shown in figure 5, with the helical and rotational quantum numbers κ and n as $n = 0, 1$ and $\kappa \in [0, \pi]$. In the neighborhood of $(\kappa, n) = (0, 0)$, there are two zero-frequency modes, TW and LA, with acoustic velocities of $C_{\mathrm{TW}} = 13.6$ km s^{-1} and $C_{\mathrm{LA}} = 20.7$ km s^{-1}, respectively. It is interesting to find that C_{TW} is much smaller than that in the graphite plane. This effect is expected to be measured in experiments with technical developments. The frequencies of the RBM, the $\vec{e}_r$ optical (OP) mode, the $\vec{e}_\phi$ OP mode and the $\vec{e}_z$ OP mode are calculated to be 538.6, 1081.5, 1544.2 and 1487.7 cm^{-1}, respectively. At $(\kappa, n) = \pm(\alpha, 1)$ with $\alpha = 2.01$ rad, there are two transverse acoustic modes—i.e. the flexure modes—with parabolic dispersions of $\omega^2 = \beta^2(\kappa \mp \alpha)^4$ in the low-frequency limits. These are the consequence of the rotational invariance of our vibration potential [48, 49].

For tubes with diameter larger than approximately 8 Å where the curvature effect dies away, the calculated frequencies (figure 4), the sound velocities for various vibration modes, and even the bond length (figure 3) etc are in accord with those of tubes of ideal geometry [49]. We notice that the slight difference in force constants between the present paper and [49] have no substantial effect on the lattice vibrational properties.

Although the lattice structure for the relaxed narrow SWCNTs deviates from that of the ideal geometry considerably, the chiral index (n_1, n_2) for the relaxed SWCNTs retains the symmetry information inherited from the hexagonal planar lattice sheet. As one might expect, our calculation verifies that various physical quantities can be expanded in terms of $\cos 3n\theta$ and $\sin 3n\theta$, $n = 1, 2, \ldots$, with the same expansion forms as those of the ideal geometry, in which θ is the chiral angle defined for the corresponding tube with ideal geometry as $\theta = \arctan \frac{\sqrt{3}n_2}{2n_1+n_2}$. As an example, in table 5 we show our fitted polarization vectors for the RBM and two optical modes in the tangential plane at $(\kappa, n) = (0, 0)$. The corresponding coefficients are shown to be almost the same as those in table 4 of [49].

4. Young's modulus and the Poisson ratio

The relaxed lattice configuration provides itself as the proper minimum of the total potential energy. In particular, the equilibrium lattice configuration for the loaded SWCNTs can also be performed, with the result that the calculation of various strain-induced physical quantities such as Young's modulus and the Poisson ratio can be carried out straightforwardly. Among the GMVs, h and h' are variables of the longitudinal degrees of freedom, while r, α and α' are variables of peripheral degrees of freedom. However, the experimentally measured longitudinal stretching should correspond to variable h, while the variable h' essentially describes the microscopic in-cell displacement. Young's modulus for the SWCNTs are introduced as:

$$Y = \left.\frac{\partial^2 E}{\partial \varepsilon_{11}^2}\right|_{\text{zero stress except the } (z,z) \text{ component}} \tag{12}$$

where $\varepsilon_{11} = \frac{\Delta h}{h}$ is the longitudinal strain, and the derivatives are taken with all the other GMVs r, α, α' and h' being freely relaxed, which corresponds to the boundary condition that all the components of the stress tensor are zero except for the (z, z) component. We stress that such a calculation of Young's

Table 6. The large-diameter limits for Young's modulus and the Poisson ratio from our calculation and other existing results are compared with the experiment data.

	Experiment [51]	Our work	Theory[a]	Theory[b]	Theory[c]
Y (eV)	56.43	56.3	60	69	53.3
μ	0.17	0.166	0.19	0.25	0.277

[a] The *ab initio* method [21].
[b] The tight-binding approximation [29].
[c] The force constant model [31].

modulus for the cylindrical lattice sheet is consistent with the classical definition of Young's modulus in the continuum limit [50]. Accordingly, the Poisson ratio

$$\mu = \left|\frac{\varepsilon_{22}}{\varepsilon_{11}}\right|_{\text{zero stress except the } (z,z) \text{ component}}, \qquad (13)$$

with ε_{22} being the peripheral strain induced under the same condition as explained above.

The calculated Young's modulus and Poisson ratio for various narrow SWCNTs can be fitted well as functions of the radius r and chiral angle θ,

$$Y = 56.3 - \frac{15.1 + 21.8\cos 6\theta}{r^2}, \qquad (14)$$

$$\mu = 0.166 + \frac{0.235 + 0.246\cos 6\theta}{r^2}, \qquad (15)$$

where Y is in the unit of eV, r is in the range [1. 3, 10] Å, θ is the chiral angle defined for the corresponding SWCNT with ideal geometry, as explained in the previous section, and the relative fitting error is kept less than 1×10^{-3}. As shown in equations (14) and (15), Young's modulus and the Poisson ratio in the large-diameter limit have values of 56.3 eV and 0.166 eV, respectively, which are in good agreement with the experimental results for graphite [51] (see table 6). In the case of narrow tubes, they are significantly chirality-dependent. For example, the Young's modulus of three SWCNTs (3, 3), (4, 2), and (5, 0), calculated as 57.74, 54.94, and 49.26, are considerably different from each other, although they have almost the same diameter.

Furthermore, we display the radius dependence of Young's modulus in figure 6 for two species SWCNTs: armchair tubes (n, n), and zigzag tubes $(n, 0)$. This shows clearly that the Young's modulus of armchair tubes decreases with increasing tube diameter and always takes values larger than that for planar graphite. Meanwhile, for zigzag tubes it exhibits contrary behavior, i.e. increases with increasing diameter and maintains a value always below that for a graphene sheet. It was reported in [26] that, among 27 samples of carbon nanotubes, some of them are measured to have a Young's modulus higher than that of bulk graphite. Meanwhile, to our knowledge, most of the existing theoretical estimations [52] can only provide values of Young's modulus less than that for a graphene sheet for any kind of SWCNTs. Our calculation provides evidence that armchair tubes are stiffer, while zigzag tubes are softer due to their chirality-dependence.

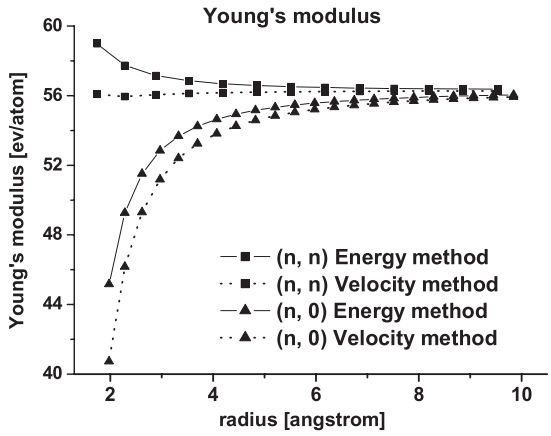

Figure 6. The Young's modulus for armchair and zigzag tubes. The lines are calculated from the second derivatives of the energy per atom with respect to the uniform strain along the tubule axis direction. Also, the dashed lines are calculated from equation (16) using the velocity method.

It is known that, following the elasticity theory of the continuum medium, Young's modulus as well as the Poisson ratio can be derived from the relevant sound velocities [37, 50],

$$Y = \rho * V_L^2, \qquad (16)$$

$$\mu = 0.5 * \left(\frac{V_L}{V_T}\right)^2 - 1, \qquad (17)$$

where the two expressions are also referenced to the boundary condition of only the (z, z) component of the stress tensor being non-zero. Therefore, we may calculate Young's modulus and the Poisson ratio from the relevant sound velocities obtained in the last section shown in figure 6 for comparison. We emphasize that the Young's modulus (Poisson ratio) calculated from the strain energy following equations (12) and (13) and those calculated from the sound velocities following equations (16) and (17) are essentially two distinct independent calculations. The former is in the sense of a microscopic calculation, following from the total potential energy equations (4)–(8), while the latter is a sort of macroscopic calculation with the sound velocities as its input, although this is provided by the microscopic vibrational energy (introduced in section 3). We can see from figure 6, for each of the two species of SWCNT (n, n) and $(n, 0)$, that the Young's moduli produced by the two kinds of calculations approach each other as the radius increases and have the same $r \to \infty$ limit as the experimental Young's modulus for graphite. Such

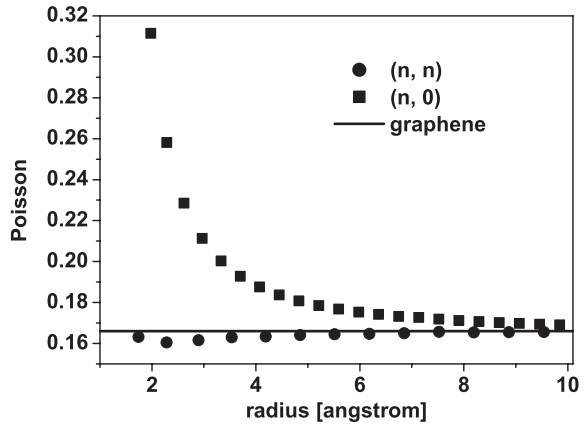

Figure 7. The Poisson ratio for different armchair and zigzag tubes.

a result arises from the intrinsic consistency between our total potential energy expression and that of the vibrational energy. The difference between the two kinds of calculations becomes apparent when the tube radius decreases. We understand such a phenomenon as the calculation following from the theory of elasticity being macroscopic in nature, which would result in failure for ultra-narrow tubes.

In figure 7, we show the calculated Poisson ratios for armchair (n, n) and zigzag $(n, 0)$ tubes as a function of radius. The values of the Poisson ratio are in the order such that those for a zigzag tube are the largest and those for an armchair tube are the smallest. This is consistent with the corresponding result of *ab initio* calculations [21].

5. Conclusions

In this paper, we propose a lattice dynamic treatment for the total potential energy of SWCNTs which is, apart from a parameter for the nonlinear effects, extracted from the vibrational energy of the planar graphene sheet. It is encouraging that such a quadratic form applies not only for SWCNTs of large radius but also to narrow SWCNTs in satisfaction with the inclusion of the nonlinear parameter. The modality of the lattice atoms, even for cases with a severe curvature effect, can be properly characterized by the six force constants.

Based upon the proposal, we investigated systematically the relaxed lattice configuration for narrow SWCNTs, the strain energy, Young's modulus and the Poisson ratio, as well as the lattice vibrational properties with respect to the relaxed equilibrium tubule structure using the same set of force constants, independent of the tube structure. In particular, with the application of GMVs we have not only successfully extended the locally introduced total potential energy to the whole tube, but we have also made the lattice dynamics for SWCNTs with relaxed geometry treatable. Comparing with the corresponding results obtained from tubes with the ideal geometry, we have verified that the relaxation effect makes the bond length longer and the frequencies of various optical vibrational modes softer. Moreover, our approach not only deduces the proper large-diameter limit values of Young's modulus and the Poisson ratio, but also provides strong evidence that SWCNTs with different chirality could be stiffer or softer than the planar graphene sheet. The calculated RBM and optical modes in the tubule's tangential plane are also in good agreement with the experimental measurements. In addition, we realized that the chiral symmetry-based general expansion formulas for different physical quantities survive for SWCNTs with relaxed geometry, in the sense that they replace the chiral angle with its counterpart defined in tubes of ideal geometry.

References

[1] Iijima S 1991 *Nature* **354** 56
[2] Saito R, Dresselhaus G and Dresselhaus M S 1998 *Physical Properties of Carbon Nanotubes* (London: Imperial College Press)
[3] Nikolaev P, Bronikowski M J, Bradley R K, Rohmund F, Colbert D T, Smith K A and Smalley R E 1999 *Chem. Phys. Lett.* **313** 91
[4] Tang Z K, Sun H D, Wang J, Chen J and Li G 1998 *Appl. Phys. Lett.* **73** 2287
[5] Wang N, Tang Z K, Li G D and Chen J S 2000 *Nature* **408** 50
[6] Li Z M, Tang Z K, Liu H J, Wang N, Chan C T, Saito R, Okada S, Li G D, Chen J S, Nagasawa N and Tsuda S 2001 *Phys. Rev. Lett.* **87** 127401
[7] Chan Y F, Peng H Y, Tang Z K and Wang N 2003 *Chem. Phys. Lett.* **369** 541
[8] Li Z M, Tang Z K, Siu G G and Bozovic I 2004 *Appl. Phys. Lett.* **84** 4101
[9] Zhao X, Liu Y, Inoue S, Suzuki T, Jones R O and Ando Y 2004 *Phys. Rev. Lett.* **92** 125502
[10] Cabria I, Mintmire J W and White C T 2003 *Phys. Rev.* B **67** 121406(R)
[11] Milošević I, Dobardžić E and Damnjanović M 2005 *Phys. Rev.* B **72** 085426
[12] Li G D, Tang Z K, Wang N and Chen J S 2002 *Carbon* **40** 917
[13] Sun H D, Tang Z K, CHen J and Li G 1999 *Solid State Commun.* **109** 365
[14] Jorio A, Souza Filho A G, Dresselhaus G, Dresselhaus M S, Righi A, Matinaga F M, Dantas M S S, Pimenta M A, Mendes Filho J, Li Z M, Tang Z K and Saito R 2002 *Chem. Phys. Lett.* **351** 27
[15] Launois P, Moret R, Le Bolloch D, Albouy P A, Tang Z K, Li G and Chen J 2000 *Solid State Commun.* **116** 99
[16] Tang Z K, Sun H D and Wang J 2000 *Physica* B **279** 200
[17] Hulman M, Kuzmany H, Dubay O, Kresse G, Li L and Tang Z K 2003 *J. Chem. Phys.* **119** 3384
[18] White C T, Robertson D H and Mintmire J W 1993 *Phys. Rev.* B **47** 5485
[19] Kürti J, Kresse G and Kuzmany H 1998 *Phys. Rev.* B **58** R8869
[20] Lianxi S and Jackie L 2005 *Phys. Rev.* B **71** 165427
[21] Daniel S, Emilio A, José M S, Angel R and Pablo O 1999 *Phys. Rev.* B **59** 12678
[22] Popov V N, Henrard L and Lambin P 2005 *Phys. Rev.* B **72** 035436
[23] Wong E W, Sheehan P E and Lieber C M 1997 *Science* **277** 1971
[24] Tombler T W, Zhou C, Kong J, Dai H, Liu L, Jayanthi C S, Tang M and Wu S Y 2000 *Nature* **405** 769
[25] Treacy M M J, Ebbesen T W and Gilson J M 1996 *Nature* **381** 678
[26] Krishnan A, Dujardin E, Ebbesen T W, Yianilos P N and Treacy M M J 1998 *Phys. Rev.* B **58** 14 013
[27] Van Lier G, Van Alsenoy C, Van Doren V and Geerlings P 2000 *Chem. Phys. Lett.* **326** 181
[28] Zhou G, Duan W and Gu B 2001 *Chem. Phys. Lett.* **333** 344

[29] Hernández E, Goze C, Bernier P and Rubio A 1998 *Phys. Rev. Lett.* **80** 4502
[30] Molina J M, Savinsky S S and Khokhriakov N V 1996 *J. Chem. Phys.* **104** 4652
[31] Lu J P 1997 *Phys. Rev. Lett.* **79** 1297
[32] Zhou X, Zhou J and Ou-Yang Z-C 2002 *Phys. Rev.* B **62** 13692
[33] Yakobson B I, Brabec C J and Bernholc J 1996 *Phys. Rev. Lett.* **76** 2511
[34] Zhan-chun T and Zhong-can O-Y 2002 *Phys. Rev.* B **65** 233407
[35] Pantano A, Boyce M C and Parks D M 2003 *Phys. Rev. Lett.* **91** 145504
[36] Wang L, Zheng Q S, Liu J Z and Jiang Q 2005 *Phys. Rev. Lett.* **95** 105501
[37] Popov V N, Van Doren V E and Balkanski M 2000 *Phys. Rev.* B **61** 3078
[38] Shen L and Li J 2004 *Phys. Rev.* B **69** 045414
[39] Tienchong C *et al* 2005 *Appl. Phys. Lett.* **87** 251929
[40] Robertson D H, Brenner D W and Mintmire J W 1992 *Phys. Rev.* B **45** 12592(R)
[41] Chang T C and Gao H J 2003 *J. Mech. Phys. Solids* **51** 1059
[42] Mori H, Hirai Y, Ogata S, Akita S and Nakayama Y 2005 *Japan. J. Appl. Phys.* **44** L1307
[43] Aizawa T, Souda R, Otani S, Ishizawa Y and Oshima C 1990 *Phys. Rev.* B **42** 11469
Aizawa T, Souda R, Otani S, Ishizawa Y and Oshima C 1991 *Phys. Rev.* B **43** 12060 (erratum)
[44] Brenner D W 1990 *Phys. Rev.* B **42** 9458
[45] Alon Ofir E 2001 *Phys. Rev.* B **63** 201403(R)
[46] Paillet M, Michel T, Meyer J C, Popov V N, Henrard L, Roth S and Sauvajol J L 2006 *Phys. Rev. Lett.* **96** 257401
[47] Meyer J C, Matthieu P, Thierry M, Alain M, Anita N, Suesberg G S, Siegmar R and Jean-Louis S 2005 *Phys. Rev. Lett.* **95** 217401
[48] Mahan G D and Jeon G S 2004 *Phys. Rev.* B **70** 075405
[49] Jiang J W, Tang H, Wang B S and Su Z B 2006 *Phys. Rev.* B **73** 235434
[50] Landau L D and Lifshitz E M 1995 *Theory of Elasticity* (Oxford: Pergamon)
[51] Blakslee O L, Proctor D G, Seldin E J, Spence G B and Weng T 1970 *J. Appl. Phys.* **41** 3373
[52] Nan Yao and Vincenzo Lordi 1998 *J. Appl. Phys.* **84** 1939
This work was referred by Xiao T and Liao K 2002 *Phys. Rev.* B **66** 153407